RSC Sustainability

ROYAL SOCIETY OF CHEMISTRY

PAPER

View Article Online
View Journal | View Issue

Cite this: *RSC Sustainability*, 2025, **3**, 4622

Mechanical, barrier, and photodegradation properties of biodegradable PLA-based blend films

Ainhoa Fernández-Tena, [a] Jorge L. Olmedo-Martínez, *[b] Marcos A. Sabino G., [c] Elizabeth Collinson, [d] Juan V. López, [e] Lourdes Irusta, [a] Alba González, [a] Antxon Martínez de Ilarduya, [f] Gonzalo Guerrica-Echevarria, [a] Nora Aranburu [a] and Alejandro J. Müller *[ag]

In this work, films based on blends of polylactide (PLA), poly(ε-caprolactone), (PCL), and the compatibilizer ElvaloyPTW were prepared by blown film extrusion; neat PLA was used as a reference material. Adding 30% PCL to PLA resulted in films with decreased modulus, yield strength, and tear resistance. However, when ElvaloyPTW was added to the 70/30 PLA/PCL blend, films featuring high ductility and improved gas barrier properties were achieved. The photodegradation of blown films based on PLA/PCL (100/0/0 and 70/30/0 wt%) and PLA/PCL/c (c = compatibilizer (ElvaloyPTW), 70/30/3 wt%) blends was comprehensively investigated under accelerated conditions using a xenon arc lamp for up to 168 h of UV irradiation. The photo-degraded samples were characterized using gel permeation chromatography (GPC), ^{1}H-NMR, FTIR-ATR, thermogravimetric analysis (TGA), polarized light optical microscopy (PLOM), and differential scanning calorimetry (DSC). The results indicate that the photodegradation of PLA/PCL/c films proceeds *via* a bulk erosion mechanism. This suggests that UV penetrates the specimens with no significant reduction in intensity, irrespective of the polymer blends' chemical structure and crystallinity. PLA and PCL chains were susceptible to photodegradation even within the crystalline regions; however, their photodegradability was lower in the crystals than in the amorphous regions. A significant decrease in molecular weight was observed with photodegradation time. The combined results of FTIR and thermal analysis allowed us to establish that the PLA phase in the blends experiences a much faster degradation rate in the presence of PCL and/or PCL/compatibilizer. Finally, the effect of photodegradation increased the crystallization rate of PLA and affected the morphology of PLA spherulites.

Received 20th June 2025
Accepted 5th August 2025

DOI: 10.1039/d5su00454c

rsc.li/rscsus

Sustainability spotlight

Our research focuses on the photodegradation of PLA/PCL polymer blends, offering a promising pathway toward sustainable material design. By enhancing the degradability of these biopolymers under light exposure, we aim to reduce long-term environmental persistence of plastics. This work directly supports the United Nations Sustainable Development Goals, particularly SDG 12 (Responsible Consumption and Production) and SDG 13 (Climate Action). Our approach aligns with circular economy principles, emphasizing renewable sources and end-of-life biodegradability. We believe that scientific innovation plays a key role in building a more sustainable future, and we're proud to contribute to this mission through practical, scalable solutions. By spotlighting this work in *RCS Sustainability*, we hope to inspire further collaboration in green materials research.

[a]*POLYMAT and Department of Polymers and Advanced Materials: Physics, Chemistry and Technology, Faculty of Chemistry, University of the Basque Country UPV/EHU, Paseo Manuel de Lardizabal 3, Donostia-San Sebastián, 20018, Spain. E-mail: alejandrojesus.muller@ehu.es*

[b]*Universidade da Coruña, Campus Industrial de Ferrol, CITENI, Campus de Esteiro S/N, Ferrol, 15403, Spain. E-mail: jorge.olmedo.martinez@gmail.com*

[c]*B5IDA Research Group, Department of Chemistry, Simón Bolivar University, Aptdo. 89000, Caracas 1080-A, Venezuela*

[d]*University of Alabama, Department of Chemical and Biological Engineering, Tuscaloosa, Alabama 35487-0203, USA*

[e]*USB Polymer Group, Department of Materials Science, Simón Bolívar University, Aptdo. 89000, Caracas 1080-A, Venezuela*

[f]*Departament d'Enginyeria Química, Universitat Politècnica de Catalunya, ETSEIB, Diagonal 647, Barcelona, 08028, Spain*

[g]*IKERBASQUE, Basque Foundation for Science, Plaza Euskadi 5, 48009, Spain*

Introduction

As is well known, traditional non-degradable plastics have led to alarming solid waste management and pollution problems. Among the industrial sectors that supply plastic waste to the environment, the packaging industry generates the highest volume of global plastic waste. Prompted by this environmental issue, the interest in biodegradable packaging materials with suitable physical, mechanical, and barrier properties has increased significantly over the last decade.[1,2] As a biobased and compostable polymer, poly(lactide) (PLA) is a potential alternative to conventional non-degradable polymers for packaging applications.[2,3] Knowing how polymers degrade under different

environmental conditions is essential in this context. Regarding PLA, most previous studies have focused on enzymatic and microbial degradation, while fewer studies can be found in the literature related to its photodegradation mechanism.[1] Nevertheless, various studies have been published in this respect,[4–10] which describe the photodegradation of PLA through photolytic, photo-oxidative, and/or Norrish I and II-type mechanisms.[4–6,10]

However, PLA is characterized by its fragility, which results in low ductility and low tear and impact resistance in the case of films. Moreover, the application of PLA in large-scale processes like blown film extrusion is limited due to its low melt strength.[11,12] PLA's properties and processing window can be improved by blending it with more flexible polymers, such as poly(ε-caprolactone) (PCL). Small amounts of PCL (~10 wt%) have proved to be enough to increase the elongation at break of PLA dramatically, and the biodegradable nature of PCL helps maintain PLA's eco-friendly character.[13] Although the properties of PLA-based blends have been extensively studied in the literature, little attention has been given to assessing the impact of photodegradation on the crystallization rate of PLA.[14,15] Moreover, due to the poor miscibility between PCL and PLA, a third component can be added to improve the interfacial interactions between PLA and PCL phases.[11,16] The intrinsic characteristics of the second and third components, the degree of crystallinity of the polymers, and the morphology created can significantly alter the gas barrier properties of the films. Besides, the degradation behavior of PLA in the resulting blends may differ from that of the neat polymer.

Several papers have focused on the compatibilization of PLA/PCL blends with PLA-PCL[17,18] block copolymers, MA grafted PLA,[19] or other compatibilizers such as methylene diphenyl diisocyanate (MDI).[20] Nevertheless, in this study, ElvaloyPTW was employed as a compatibilizing agent due to its molecular structure, which includes glycidyl methacrylate (GMA) and acrylate groups; these groups can react with the functional end groups of PLA and PCL, improving compatibility and adhesion between the phases.[21] A comparison between ElvaloyPTW and six other similar compatibilizers was reported in a previous study by us, where it was concluded that ElvaloyPTW was the most effective among the compatibilizers employed for PLA/PCL blends. These polymer blends offer promising applications in biomedical innovation,[22] food and pharmaceutical packaging[23] with enhanced mechanical properties and biodegradability,[24,25] and in industrial uses such as 3D printing filaments.[26,27]

The present work demonstrates how adding a soft polymer (PCL) and a compatibilizer (ElvaloyPTW) can affect the properties and photodegradation of PLA in blown films. The influence of UV irradiation on the chemical stability of the films, as well as the effect of UV exposure over time (under experimentally accelerated aging conditions) on the photodegradation process of PLA, has been analyzed. Furthermore, photodegradation-induced chain scission strongly affects the crystallization capacity of the PLA component.

Experimental part

Materials

A PDLLA with 1.2–1.6% D-isomer (PLA Ingeo Biopolymer 4032D) was supplied by NatureWorks (Minneapolis, MN, USA) with a weight-average molecular weight of 190 kg mol^{-1}. PCL CAPA6800, with a weight-average molecular weight of 80 kg mol^{-1}, was purchased from Ingevity (North Charleston, SC, USA). The compatibilizer was a polyethylene-based copolymer (ElvaloyPTW) donated by Dow Chemicals, which possesses 28% *n*-butylacrylate and 5.3% glycidyl methacrylate.

Sample preparation

All the materials were dried overnight before melt processing to avoid moisture-induced degradation. PCL and ElvaloyPTW were dried in an oven at 40 °C, and PLA was dried in a dehumidifier at 80 °C. Before the blown film extrusion process, the blends PLA/PCL (70/30 wt%) and PLA/PCL/ElvaloyPTW (70/30 weight ratio plus 3% of the compatibilizer with respect to the total weight of the blend) were melt blended in a Collin Teach-Line ZK25 T SCD 15 twin-screw extruder (*L*/*D* ratio 18 and screw diameter 25 mm) (Ebersberg, Bavaria, Germany). As a reference, neat PLA was also extruded. Samples were named PLA/PCL/ElvaloyPTW, *i.e.*, 100/0/0, 70/30/0, and 70/30/3. In all the cases, the processing temperature and screw speed were set at 190 °C and 200 rpm, respectively. The extrudates were cooled in a water bath and pelletized.

Before the blown film extrusion process, the pellets were dried overnight in a dehumidifier at 80 °C. The films were prepared in a Collin Teach-Line E 20T single-screw extruder (Ebersberg, Bavaria, Germany; screw diameter 20 mm and *L*/*D* ratio 25 : 1) coupled to a blowing unit Collin Teach Line BL 50 T equipped with a BL-D annular die of 30 mm of diameter, an opening of 0.8 mm, a lip-type cooling ring, and a collecting and winding system. For neat PLA, the processing temperature was 220 °C, while for the two blends, 200 °C was used. In all the cases, the screw speed was 70 rpm. The blow-up ratio (BUR) and the take-up ratio (TUR) were 4 : 1 and 6, respectively. Films with a nominal thickness of 30 μm were obtained.

Photodegradation process

Films were cut into rectangular-shaped samples of dimensions 200 × 100 mm^2. The samples were placed in an irradiation chamber and UV irradiated using an accelerated photo-ageing device (Solarbox from Neurtek) (UV – with a xenon arc light source and a 300 nm filter). The irradiation process was carried out without humidity rate control in the presence of oxygen in the air. The temperature inside the irradiation chamber was kept constant at 40 °C. Films were exposed to UV irradiation for up to 168 h. The irradiated samples are denoted as PLA/PCL/ElvaloyPTW-*x*, where "*x*" indicates the irradiation time in hours.

Characterization

Tensile test. Tensile tests were performed using an Instron 5569 tensile tester (Instron, Norwood, MA, USA).

A 10 mm min^{-1} crosshead speed was used to determine the modulus, yield strength, and elongation at break. Specimens were prepared according to ASTM D-638 type V. Films were tested in two directions, *i.e.*, machine direction (MD) and transversal direction (TD). At least five specimens were tested for each reported value.

Trouser tear tests. Tear resistance was determined using an Instron 5569 tensile tester (Instron, Norwood, MA, USA), with an initial distance of 50 mm and a crosshead speed of 250 mm min^{-1}. Trouser specimens were prepared according to ASTM 1938 and were tested in both MD and TD. At least five specimens were tested for each reported value.

Barrier properties. O_2, H_2O, and CO_2 permeation were measured for the three compositions. In the case of PLA/PCL/c 70/30/3, CO_2 permeability could not be measured since the films broke during the measurements. The O_2 permeability coefficient was measured with a Mocon OX-TRAN 2/21 MH model instrument at 1 atm, 25 °C, and 0% relative humidity.

The films' water vapor transmission rate (WVTR) was determined in a Sartorius BP210D gravimetric cell. The Teflon cell with the polymeric film was placed on a balance within a temperature and humidity-controlled chamber set at 25 °C and 45–60% relative humidity. The weight loss, *i.e.*, the water loss, was measured over time. The WVTR (g mm m^{-2} day^{-1}) was determined by calculating the slope of the weight loss *vs.* time plot using eqn (1):[28]

$$\mathrm{WVTR} = \frac{m \times l}{A(a_{\mathrm{int}} - a_{\mathrm{ext}})} \quad (1)$$

where m (mass flux) is the slope of the curve, l is the thickness of the film, A is the effective mass transfer area between the film and the water vapor (2.54 cm^2), a_{int} is the water vapor activity in the headspace of the cell (considered to be equal to 1), and a_{ext} is the water vapor activity in the chamber (assumed to be equal to the relative humidity in the case of water, about 0.45–0.60).

The permeability to CO_2 was measured at 25 °C and 1 atm in a manometric permeation cell. The pressure was registered in a computer using the Press Aquirer V0.2 software. Circular films of 1.8 cm^2 were used to perform the measurements.

H_2O and CO_2 permeation measurements were repeated three times for each composition to obtain an average value, whereas O_2 permeation measurements were repeated twice.

Gel permeation chromatography (GPC). The number (M_n) and weight (M_w) average molecular weights and dispersity index ($Đ$) were determined using a Waters GPC instrument equipped with refractive index (RI) and ultraviolet (UV) detectors. Approximately 1–2 mg of the samples were dissolved in 1 mL of chloroform and filtered with a 0.22 μm PTFE filter. 100 μL of these solutions were injected into the system and eluted with chloroform at a 0.5 mL min^{-1} flow rate. HR5E and HR2 Waters linear Styragel columns (7.8 × 300 mm, pore size 10^3–10^4 Å) packed with crosslinked polystyrene and protected with pre-column were used. Polystyrene (PS) standards with narrow molecular weight distributions were employed to generate the calibration curve.

Fourier transform infrared-attenuated total reflectance (FTIR-ATR) spectroscopy. The infrared spectra of the films before and after irradiation were recorded on a Nicolet 6700 FTIR spectrometer coupled to an ATR accessory (Golden Gate) (Thermo Fisher Scientific, Waltham, MA, USA). Spectra were recorded with a resolution of 4 cm^{-1}. The final spectra were the average over 32 scans. The analysis was carried out by placing the face of the sample exposed to the UV lamp on the ATR.

Nuclear magnetic resonance (^{1}H-NMR). ^{1}H-NMR spectra were recorded on a Bruker AMX-300 spectrometer at 25 °C operated at 300.1 MHz. Around 10 mg of the sample was dissolved in 1 mL of chloroform ($CDCl_3$). 640 scans were accumulated for recording these spectra using tetramethylsilane (TMS) as an internal reference. These results are presented in SI (Fig. S1–S3).

Thermal gravimetric analysis (TGA). Thermogravimetric data were collected on a thermobalance TA instrument TGA-Q500 from 50 to 600 °C under nitrogen at a 60 mL min^{-1} flow rate. The heating rate was set at 10 °C min^{-1}. These plots are presented in the SI (Fig. S4).

Differential scanning calorimetry (DSC). Calorimetric studies were carried out in a TA DSC25 differential scanning calorimeter. Measurements were performed under ultrahigh-purity nitrogen as an inert atmosphere with a 20 mL min^{-1} flow rate. The calorimeter was calibrated using indium and tin standards. Approximately 3–5 mg of the samples were placed into the DSC pans for the measurements.

Non-isothermal DSC measurements were performed: (1) the samples were heated from room temperature to 200 °C at 20 °C min^{-1} (first heating), and (2) the thermal history was erased by keeping the sample at 200 °C for 3 min. Then, the samples were cooled to −50 °C and heated to 200 °C at 20 °C min^{-1}. From these cooling and second heating scans, the crystallization temperature (T_c), the cold crystallization temperature (T_{cc}), the melting temperature (T_m), and the enthalpies corresponding to each transition were obtained. The degree of crystallinity (X_c) of PLA and PCL was calculated according to eqn (2):[29]

$$X_c = \frac{\Delta H_m - \Delta H_{cc}}{\Delta H_m^0 \times w_f} \quad (2)$$

where ΔH_m and ΔH_{cc} are the measured melting and cold crystallization enthalpies, respectively, ΔH_m^0 is the melting enthalpy of completely crystalline PLA (93.6 J g^{-1} (ref. 13 and 29)) or PCL (139.5 J g^{-1} (ref. 30 and 31)), and w_f represents the weight fraction of PLA or PCL in the blend.

For the isothermal crystallization experiments, the T_c range employed for each sample was determined using the methodology recommended by Lorenzo *et al.*[32]

Once the T_c values to be employed were determined, the samples were evaluated as follows: (1) heating from 25 to 200 °C at 20 °C min^{-1}; (2) holding at 200 °C for 3 min; (3) cooling to T_c at 60 °C min^{-1}; (4) holding at T_c during 15–40 min to allow crystallization to saturate; and (5) heating from T_c to 200 °C at 20 °C min^{-1} to register the melting behavior after the isothermal crystallization.

Spherulitic growth rate. The spherulitic growth rate was measured using an OLYMPUS BX51 polarized light microscope fitted with an OLYMPUS SC50 camera and a Mettler FP82HT hot

stage with liquid nitrogen cooling capability. The samples were placed between two glass slides and heated 20 °C above their melting temperature (using the DSC measurements as the reference) to form a thin film. Then, they were kept at this temperature for 3 minutes to erase thermal history. The samples were then cooled at 50 °C min^{-1} to a temperature at which the spherulites began to appear, and the growth of the spherulite was followed isothermally as a function of time by recording micrographs. This procedure was repeated for 10 different temperatures.

Results

Characterization of neat films

Table 1 summarizes the parameters determined from the first DSC heating scans for the PLA and the PLA phase within the blends. Since the melting of PCL crystals occurs in the same temperature range as the glass transition of PLA, the T_m, and X_c of PCL could not be determined. Moreover, no signal corresponding to the compatibilizer was observed.

70/30 PLA/PCL blends are immiscible and exhibit a sea island morphology when compression molded, with PCL droplets well dispersed in a PLA matrix. The PCL droplets can be elongated or deformed depending on the processing conditions and can transition to a co-continuous morphology (see, for instance, our previous work cited in ref. 21, where similar samples were employed).

During the first heating scan of the as-extruded films, neat PLA shows an exothermic peak at 113 °C, corresponding to a cold crystallization transition, and a melting peak at 167.4 °C (Fig. S5). As a result of the low crystallization rate of PLA and the fast cooling rates applied during the manufacturing of the films, PLA displays a negligible crystallinity degree, X_c is approximately 0%. When PCL is added to PLA, the T_{cc} of PLA dramatically decreases to 90.3 °C, and the X_c is enhanced up to 12%. These changes result from the nucleating effect of the PCL phase on the PLA matrix. In the case of the first heating run of the films, the nucleating effect of the PCL phase can be attributed to a surface nucleation effect of the previously crystallized PCL phase. The nucleating effect can also be obtained during cooling from the melt and, in that case, even when the PCL is in the molten state. This has been attributed in the literature to heterogeneity migration from the PCL to the PLA phase.[33,34]

The incorporation of the compatibilizer hardly varies the T_{cc} and X_c of PLA (see Table 1), suggesting that the compatibilizer has a negligible impact on the crystallization ability of PLA. Although the blends display a lower T_m compared to neat PLA, the variations are too small to establish a relationship between the T_m of PLA and the presence of PCL and the compatibilizer within the matrix. These results agree with the results obtained in our previous work,[21] where the same three compositions were prepared by injection molding.

Table 2 summarizes the mechanical parameters obtained by tensile and trouser tear tests. Films were tested in two directions, *i.e.*, machine direction (MD) and transversal direction (TD). Neat PLA films (100/0/0) display a typical brittle behavior, high modulus and strength, and low ductility and toughness. The incorporation of PCL decreased modulus, yield strength, and tear resistance, while a significant improvement in elongation at break (from 5% to 65%) and toughness (from 59 to 504 J m^{-2}) was obtained. A similar behavior was observed by Diaz *et al.*[15] for PLA/PCL blown films. However, in their case, a lower improvement in ductility was observed, and the tear resistance increased slightly with the addition of PCL. Incorporating the compatibilizer into the 70/30/3 blend improved the films' ductility and toughness to 93% and 600 J m^{-2}, respectively. At the same time, the modulus, yield strength, and tear resistance remained almost the same as in the non-compatibilized 70/30/0 blend. Overall, the mechanical properties of the films tested in the MD were higher, or almost equal, than in the TD. This effect is associated with the anisotropy of the samples, which is typically observed in blown films. The effect occurs due to the molecular orientation in the amorphous phase during the extrusion-blow molding process, where the molecular chains tend to orient along MD, leading to better mechanical properties in that direction.[12] This effect is more pronounced in PLA/PCL and PLA/PLC/c blends, probably because of the PCL soft nature and the compatibilizer facilitating the molecular orientation.

Fig. 1 shows the water vapor, oxygen, and carbon dioxide permeability values obtained in this work for the three studied films. As can be observed, the barrier properties of the films

Table 1 T_{cc}, T_m, and X_c values of PLA obtained from the first DSC heating scans

Composition	T_{cc} (°C)	T_m (°C)	X_c (PLA) (%)
PLA/PCL 100/0/0	113 ± 2	167 ± 0.9	0 ± 0
PLA/PCL 70/30/0	90 ± 0.4	166 ± 0.4	12 ± 0
PLA/PCL/c 70/30/3	88 ± 0.8	165 ± 0.4	15 ± 2

Table 2 Parameters obtained by tensile and trouser tear tests

Sample	Testing direction	Modulus (MPa)	Yield strength (MPa)	Elongation at break (%)	Toughness (J m^{-2})	Tear resistance (N mm^{-1})
PLA/PCL/c 100/0/0	MD	3460 ± 280	45 ± 6	5 ± 0.9	59 ± 10	14 ± 1
	TD	3440 ± 210	43 ± 2	10 ± 4	111 ± 57	13 ± 0.9
PLA/PCL/c 70/30/0	MD	1740 ± 240	28 ± 2	65 ± 9	504 ± 69	4.6 ± 0.7
	TD	1760 ± 230	23 ± 2	41 ± 6	283 ± 43	3.8 ± 0.5
PLA/PCL/c 70/30/3	MD	1740 ± 150	25.2 ± 2	93 ± 15	600 ± 146	4.5 ± 0.4
	TD	1400 ± 190	21 ± 2	64 ± 12	403 ± 128	3.5 ± 0.4

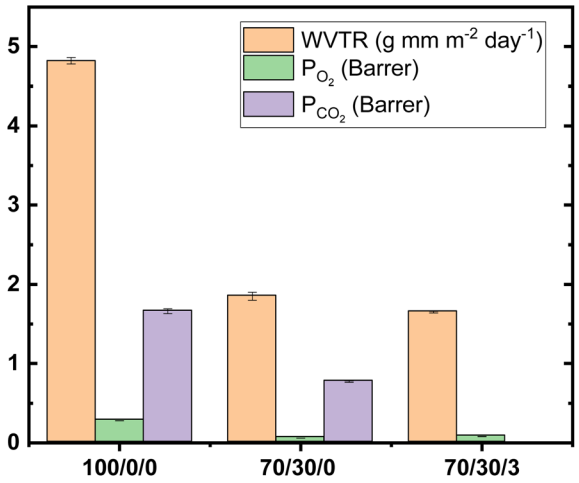

Fig. 1 Water vapor, oxygen, and carbon dioxide permeability of the films.

improved significantly with the incorporation of PCL. An even lower water vapor permeability was achieved in the compatibilized blend, while the oxygen permeability remained almost the same as the non-compatibilized PLA/PCL blend. The carbon dioxide permeability of PLA/PCL/c films could not be measured since the samples broke during the tests. The permeability results obtained in this work disagree with the values reported in the literature. Cabedo *et al.*[35] and Urquijo *et al.*[36] studied the oxygen permeability of compression-molded PLA and PLA/PCL blends, observing a decrease in the barrier properties of the blends due to the higher permeability of neat PCL. Different factors, such as the degree of crystallinity or the blend morphology, can alter the barrier properties of a blend.[37] It has to be noted that, in the referenced studies, a sea-island morphology was reported. The morphologies were observed in our previous work for similar materials,[21] and the PLA/PCL blend displayed a morphology between sea-island and co-continuous, while the PLA/PCL/c composition had a co-continuous morphology. Moreover, as shown in Table 1, the presence of the PCL increases the X_c of PLA. Besides, even though it cannot be confirmed, the X_c of PCL in the blends could also be higher thanks to the chain orientation induced by the blowing process. All these factors could be responsible for the observed better barrier properties in PLA/PCL and PLA/PCL/c blends.

Incorporating PCL and a compatibilizer like ElvaloyPTW into PLA has proved helpful in achieving a PLA-based film with high ductility and improved gas barrier properties.

Photodegradation

Fourier transform infrared spectroscopy (FT-IR). FT-IR spectroscopy is widely used to study polymer degradation processes. Fig. 2 shows the main signals relating to photo-oxidative degradation in films exposed to UV radiation for 168 hours.

FT-IR spectra for all the films show the characteristic bands for polyester as PLA and PCL (Fig. S6 shows the complete spectra): 2998 and 2949 cm^{-1} related to the C–H stretching of methyl, methylene, and methyne groups, 1745 cm^{-1} associated with the carbonyl group stretching, between 748 and 1200 cm^{-1} related to the skeletal structure of the polymer chain.[38,39]

The more relevant differences detected by FT-IR between the blends irradiated by UV at different times are shown in Fig. 2. These results show the presence of two significant changes around the carbonyl band between 1700 and 1800 cm^{-1} and the appearance of extra peaks in the 1825–1865 cm^{-1} region with degradation time (attributable to anhydride functional groups) for the photo-oxidized films (see also the Nuclear Magnetic Resonance ^{1}H-RMN results in Fig. S1). The most significant change is observed in the band of the carbonyl group, where it has been reported that the band at 1745 cm^{-1} is due to the presence of amorphous polyester, and the band at 1725 cm^{-1} is related to crystalline polyester.[40] In the case of neat PLA, it is observed that at an irradiation time of 0 h, only the peak of the amorphous phase is observed (as observed in the DSC, PLA is amorphous at room temperature (Fig. S5a)); however, when increasing the irradiation time (between 96 and 120 h), the peak related to the crystalline phase appears. This is because as photodegradation progresses, the size of the polymeric chains decreases, and crystallization gradually occurs (a process sometimes referred to in the literature as chemo-crystallization[41,42]). When irradiation increases to 144 h, the material is entirely amorphous again due to the blend's severe photodegradation.

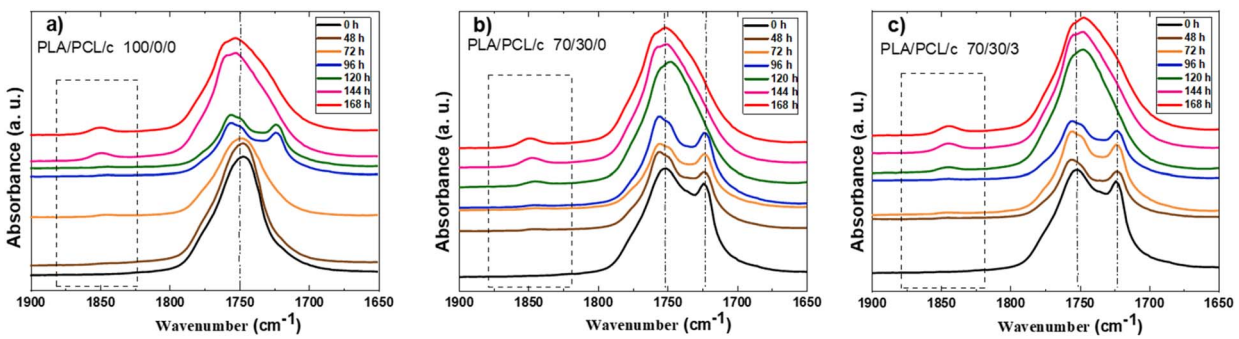

Fig. 2 FT-IR spectra of the carbonyl group band as a function of irradiation time for (a) PLA 100/0/0, (b) PLA/PCL 70/30/0, and (c) PLA/PCL/c 70/30/3.

In the case of PLA/PCL and PLA/PCL/c blends, it is observed from the time 0 h that the two characteristic carbonyl bands (that can be correlated with amorphous or semi-crystalline PLA) are found at 1745 and 1725 cm^{-1}. When increasing the irradiation time to 120 h in both cases, only the band related to the amorphous material is observed, which indicates that this UV irradiation time is sufficient to degrade and render the samples amorphous. These results align with the TGA data (see Fig. S4) and show that PLA degradation occurs faster when mixed with PCL or PLA/c, as the fully amorphous polymer signal is reached at shorter irradiation times.

Molecular weight changes caused by photodegradation measured by GPC. GPC traces of neat PLA, PLA/PCL, and PLA/PCL/c at different irradiation times are shown in Fig. 3a–c. The elution time of PLA increases significantly with irradiation time; it is also observed that the peak is much broader, which is reflected in an increase in polydispersity (Fig. 3d); this increase in polydispersity is more evident in the PCL and PCL/c blends; because these materials, as shown by TGA and FTIR, degrade more easily. It is important to note that in the case of the blends, the size exclusion chromatography measurements were performed after the complete dissolution of the blends in chloroform (which dissolves PCL, PLA, and the compatibilizing

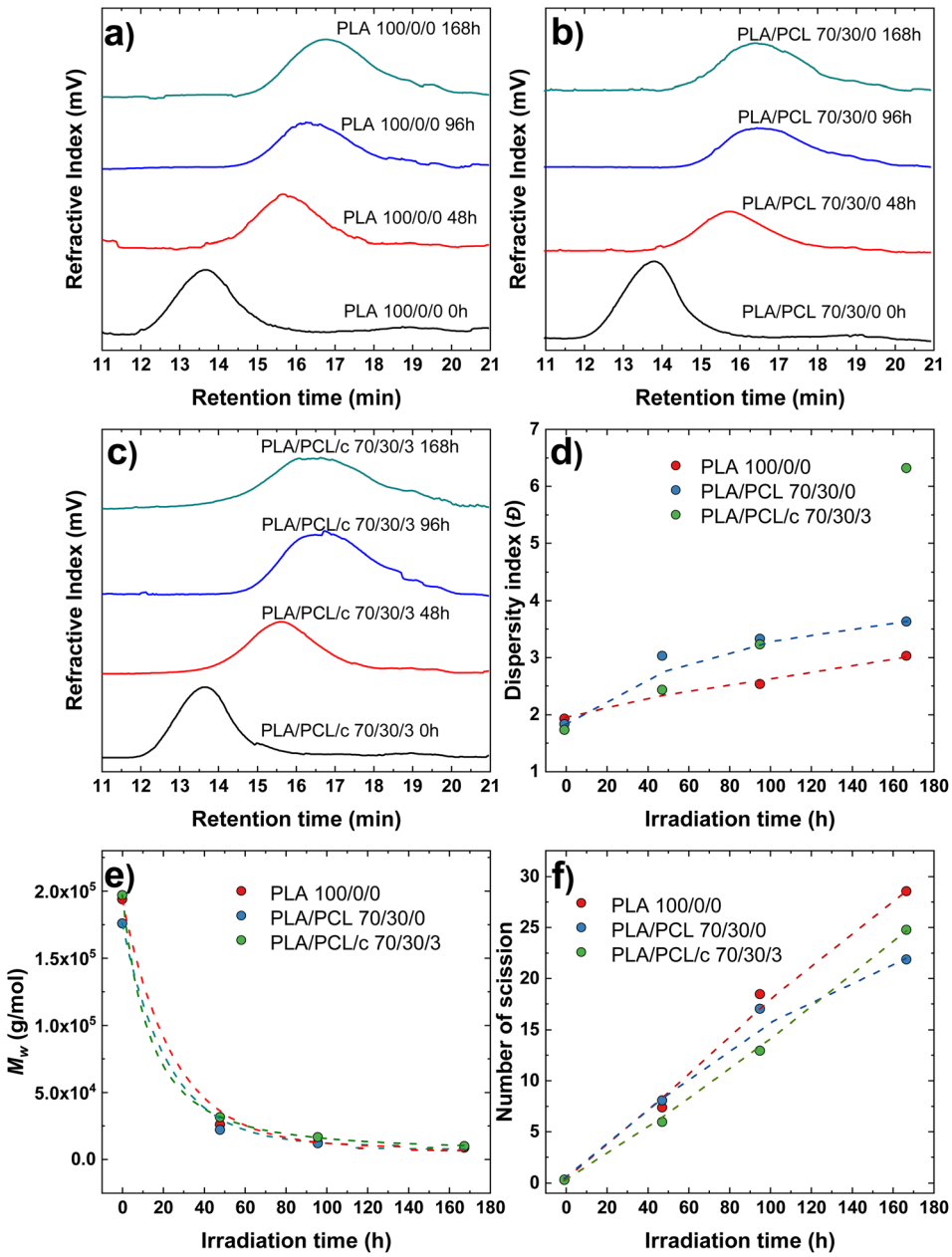

Fig. 3 (a) Refractive index for PLA samples at different irradiation times, (b) refractive index for PLA/PCL samples at different irradiation times, (c) refractive index for PLA/PLA/c samples at different irradiation times, (d) dispersity index as a function of irradiation time for all the samples, (e) average M_w as a function of irradiation time for all samples, and (f) number of scissions as a function of irradiation time for all the samples.

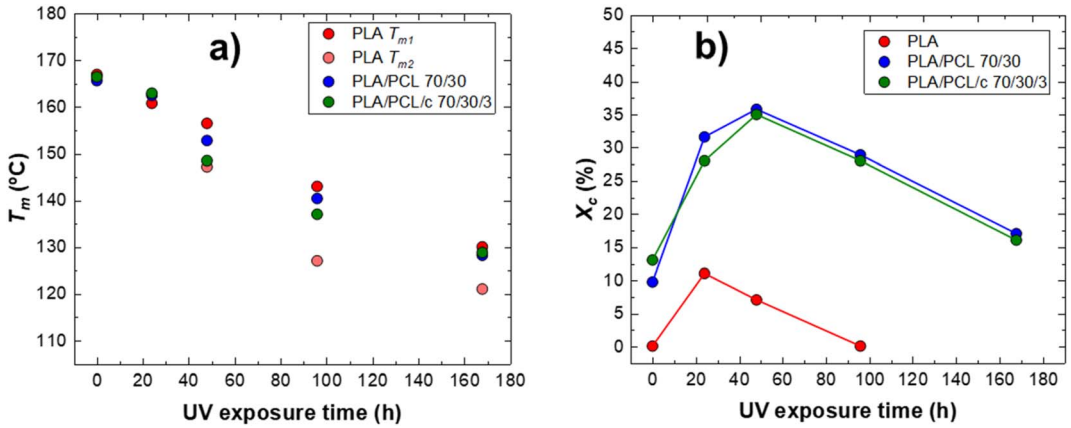

Fig. 4 (a) Melting temperature (T_m) as a function of UV exposure time for neat PLA and different blends, and (b) crystallization degree (X_c) as a function of UV exposure time for neat PLA and different blends.

agent). Thus, the measured weight average molecular weight is an average for all dissolved molecules. However, given that PLA constitutes at least 70% of the weight of the blend, the results are likely to be dominated by PLA.

As can be observed in Fig. 3e, the average M_w of the three samples suffers a rapid decrease in the first 48 h of UV exposure. Such a dramatic decrease has been ascribed to the random scission of PLA backbone chains caused by photon absorption.[43] The degradation of the PCL component is also possible, as the M_w of the blends decreases as fast as neat PLA. Between 48 h and 168 h, the M_w continues to decrease very slowly. Meanwhile, the $Đ$ increases with irradiation time. This increase is more evident in the blends rather than in neat PLA.

To analyze the relation between the drop in molecular weight and the bond cleavage, the number of cleaved bonds (S) was calculated following ref. 43 according to eqn (3):

$$S = \frac{M_0}{M_t} - 1 \quad (3)$$

where M_0 and M_t are the molecular weights of the PLA in the blend before and at irradiation time t, respectively. Fig. 3f shows that as the irradiation time increases, the number of cleaved bonds increases due to photodegradation.

Non-isothermal DSC. Non-isothermal DSC experiments were performed to determine the change in melting temperature (T_m) and crystallinity degree (X_c) of PLA in the different blends as a function of irradiation time (taken from Fig. S5). The molecular weight significantly influences the T_m and X_c of polymeric materials. Fig. 4a shows how the T_m values decrease with the UV exposure time as the molecular weight decreases. Two melting peaks related to the α and α' phases were observed in all the blends.[44] These values decreased from around 170 to 120 °C with 168 h of UV irradiation.

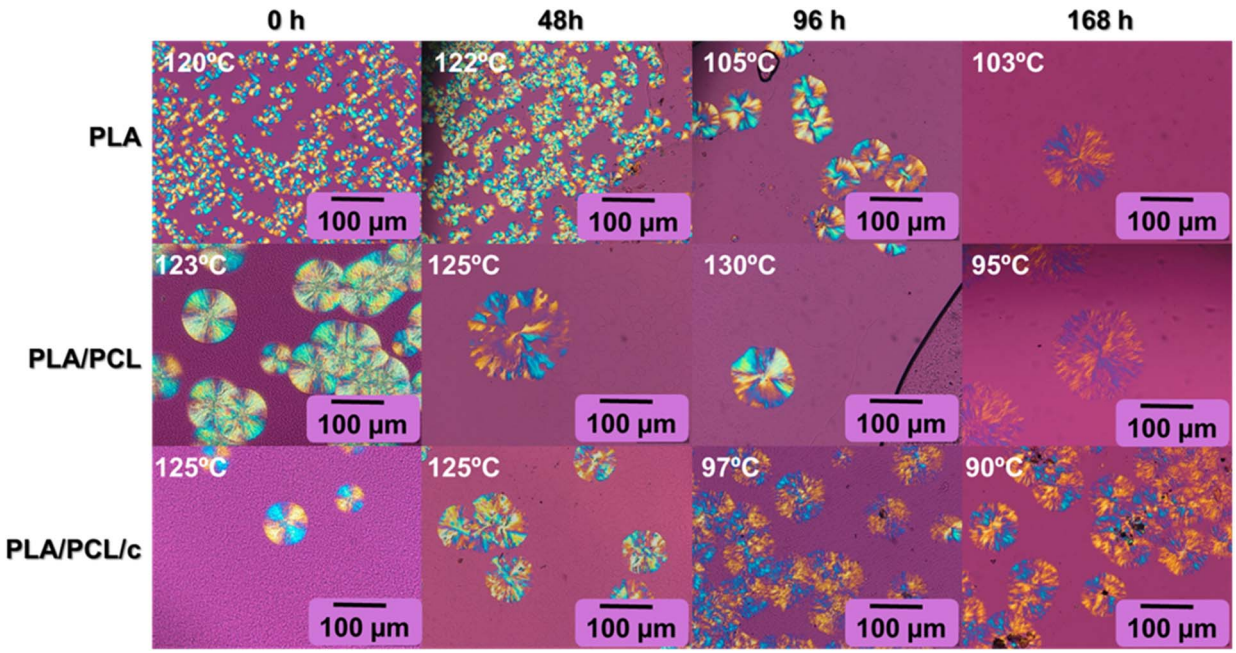

Fig. 5 PLA spherulitic morphology observed by PLOM at different irradiation times for the indicated blends.

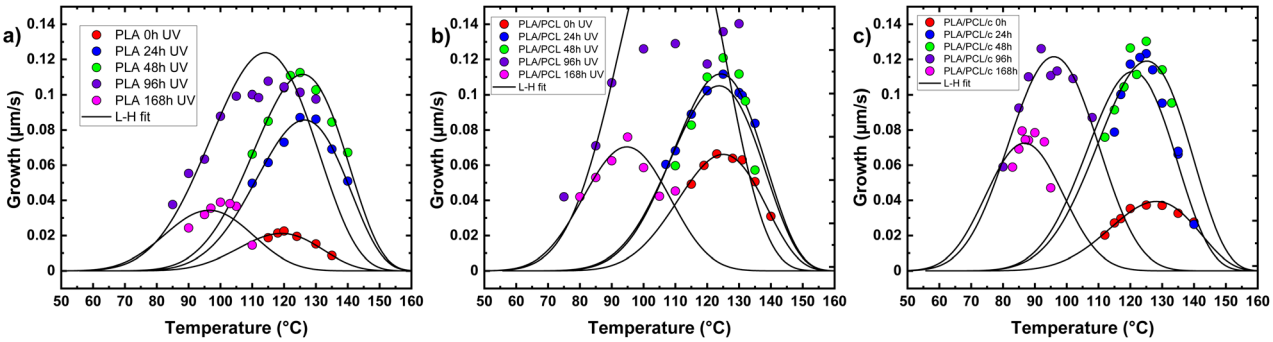

Fig. 6 Spherulitic growth rate as a function of temperature for selected irradiation times, (a) PLA 100/0/0, (b) PLA/PCL 70/30/0, and (c) PLA/PCL/c 70/30/3.

Fig. 4b shows the PLA degree of crystallinity of the samples as a function of the irradiation time (calculated using eqn (2)), calculated from the first heating scan. For PLA and PLA blends, it can be observed that up to 24 h and 48 h of irradiation, respectively, the X_c increases, and after this time, the value of X_c begins to decrease. This behavior occurs because, during the first hours of irradiation, the polymeric chains that are in the amorphous state are photodegraded. Then, they recrystallize at longer UV exposure times (*i.e.*, a chemo-crystallization effect). At even longer irradiation times, the chains in the crystalline phase can also photodegrade, which causes a decrease in the degree of crystallinity.

The SI compares the molecular weight calculated using the T_g values of PLA (only for neat PLA because, in the case of the blends, it was impossible to measure the T_g of PLA since the T_g value of PLA overlaps with the T_m of PCL) (Fig. S7) and that obtained by GPC (Fig. S8). The agreement is qualitatively satisfactory.

Morphology and spherulitic growth rate. PLA spherulite morphology can change due to degradation caused by UV irradiation time. Fig. 5 shows the spherulitic morphology for PLA and the blends at different irradiation times. We can observe well-defined PLA spherulites in the images at 0 h with Maltese-cross extinction patterns. According to the micrographs shown, which were taken with a red tint plate to exhibit retardation colors related to the presence of birefringent crystals, the PLA spherulites are negative[45–47] in all cases (*i.e.*, they appear yellow in the first and third quadrants, and blue in the second and fourth quadrants), as expected. The difference in the size and number density of spherulites may vary in each mixture due to the temperature at which the image was taken. For example, in the case of neat PLA, there is a larger number of spherulites because they were observed at 120 °C (at higher supercooling where nucleation increases), while in the case of PLA blends, they were observed at 123–125 °C. However, in this experiment, the objective was to observe possible modifications in the morphology of the spherulites. In the case of the mixtures with PCL at 48 h of irradiation, some non-birefringent circular regions are observed inside the spherulites. In this case, this indicates the presence of molten PCL droplets engulfed by the growing PLA spherulites.[48] When the irradiation time is increased even more up to 96 and 168 h, it is observed that the PLA spherulites suffer changes in their morphology due to the degradation of the chains forming the lamellar crystals, leading to a bushy type of spherulite which is more open.[45]

Polarized Light Optical Microscopy (PLOM) was also used to follow the growth of the spherulites at different crystallization temperatures and irradiation times and thus calculate the spherulitic growth rates. Fig. 6 shows the PLA spherulitic growth rate as a function of temperature for neat PLA and for the PLA component within the blends at different irradiation times. In all cases, the slowest PLA spherulitic growth rate is for the sample that has not been irradiated; then, with 24 and 48 h of irradiation, the spherulitic growth rate increases at the same

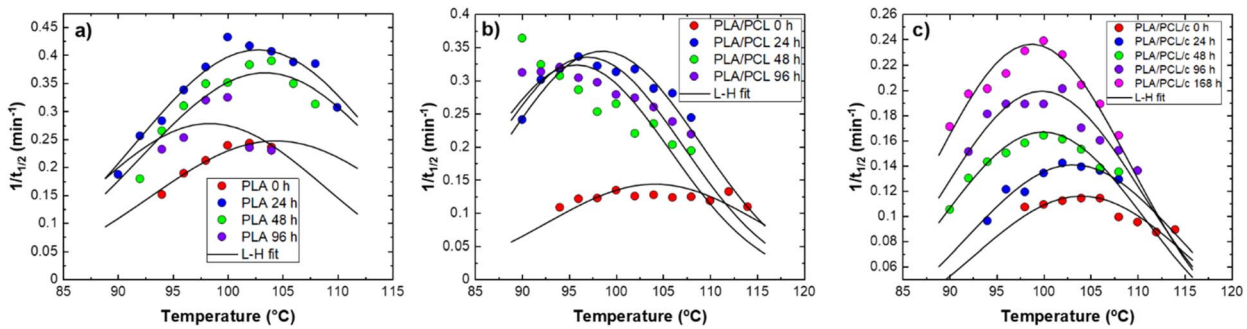

Fig. 7 Overall crystallization rate as a function of temperature for all the irradiation times, (a) PLA 100/0/0, (b) PLA/PCL 70/30/0, and (c) PLA/PCL/c 70/30/3.

crystallization temperature range. The increase in PLA growth rate is due to the decrease in molecular weight caused by photodegradation.[49,50]

The supercooling needed for spherulitic growth is increased at even higher irradiation times. The bell-shaped curve of *G versus* T_c shifts to lower temperature values as both T_g and T_m decrease. In other words, as degradation proceeds to a greater extent, the crystallization window (the interval between T_g and T_m) shifts to lower values.

As shown in Fig. 6, when comparing the samples at the same irradiation time, the crystallization temperature decreases, and the crystallization rate increases slightly. This could be because the PCL and PCL/c blends degrade faster than neat PLA.

Overall crystallization rate. DSC isothermal crystallization experiments (which include both primary nucleation and growth) were performed to study how photodegradation affects the overall crystallization rate of PLA in the different samples. Fig. 7 shows plots of the inverse of the half-crystallization time ($1/\tau_{50\%}$) as a function of crystallization temperature for all the studied materials. The main difference is that in the case of PLA and PLA/PCL, measuring the crystallization rate with 168 h of irradiation was impossible because the time for PLA to crystallize was too long to be monitored by DSC. However, it can be concluded that the photodegradation of PLA chains directly affects the crystallization rate since, as expected, the overall crystallization rate increases with degradation time.

Conclusions

Blends of PLA, PCL, and ElvaloyPTW were prepared by extrusion blowing; neat PLA was used as a reference material. Incorporating PCL decreased PLA's modulus, yield strength, and tear resistance, while a significant improvement in elongation at break was obtained from 5% to 65%. Incorporating PCL and ElvaloyPTW into PLA made the preparation of PLA-based blown films with high ductility and improved gas barrier properties possible.

The photodegradation of the prepared extrusion-blown films was first studied using FT-IR. It was possible to demonstrate that the degradation caused by UV radiation affects PLA and PCL since changes were observed in the carbonyl bands (1700–1800 cm^{-1}) as the irradiation time increased. The signal related to the crystalline part of the material (1725 cm^{-1}) disappears, and only the band characteristic of the amorphous part remains (1745 cm^{-1}). We correlated the changes in the T_g of PLA at different times of UV exposure with the decrease in the molecular weight of PLA. The results of FTIR and TGA allowed us to establish that the PLA phase in the blends experiences a much faster degradation rate when PCL and PCL/compatibilizer are present.

The compatibilizing agent (ElvaloyPTW) had no significant effect on the PLA crystallization rate in the blends. However, due to the decrease in molecular weight caused by photodegradation, both the spherulitic growth rate and the overall crystallization rate of the PLA component showed a significant increase with irradiation time.

Conflicts of interest

There are no conflicts to declare.

Data availability

Data will be made available on request.

Nuclear magnetic resonance (^{1}H-RMN) spectra, proposed mechanism of photo-oxidative degradation of PLA, thermal gravimetric analysis (TGA), complete FTIR spectra, first and second DSC scans and fit parameters of Avrami equation are presented in the SI. See DOI: **https://doi.org/10.1039/d5su00454c**.

Acknowledgements

We acknowledge the financial support from the BIODEST project; this project received funding from the European Union's Horizon 2020 research and innovation program under the Marie Skłodowska-Curie Grant Agreement No. 778092. This work has also received funding from the Basque Government through grant IT1503-22. We want to thank Dr Jason Bara from the University of Alabama for coordinating the exchange of students from his Institution to the University of the Basque Country UPV/EHU. Thanks to this exchange program, Elizabeth Collinson did a summer internship at POLYMAT and the University of the Basque Country UPV/EHU, significantly contributing to the present paper.

References

1 N. F. Zaaba and M. Jaafar, *Polym. Eng. Sci.*, 2020, **60**, 2061–2075.
2 L. K. Ncube, A. U. Ude, E. N. Ogunmuyiwa, R. Zulkifli and I. N. Beas, *Materials*, 2020, **13**, 4994.
3 R. Auras, B. Harte and S. Selke, *Macromol. Biosci.*, 2004, **4**, 835–864.
4 W. Wang, G. Ye, D. Fan, Y. Lu, P. Shi, X. Wang and B. Bateer, *Polym. Degrad. Stab.*, 2021, **194**, 109762.
5 A. V. Janorkar, A. T. Metters and D. E. Hirt, *J. Appl. Polym. Sci.*, 2007, **106**, 1042–1047.
6 H. Tsuji, Y. Echizen and Y. Nishimura, *Polym. Degrad. Stab.*, 2006, **91**, 1128–1137.
7 M. C. Mistretta, F. P. La Mantia, V. Titone, L. Botta, M. Pedeferri and M. Morreale, *J. Appl. Biomater. Funct. Mater.*, 2020, **18**, DOI: **10.1177/2280800020926653**.
8 H. Tsuji, H. Sugiyama and Y. Sato, *J. Polym. Environ.*, 2012, **20**, 706–712.
9 A. Copinet, C. Bertrand, S. Govindin, V. Coma and Y. Couturier, *Chemosphere*, 2004, **55**, 763–773.
10 S. Bocchini, K. Fukushima, A. Di Blasio, A. Fina, A. Frache and F. Geobaldo, *Biomacromolecules*, 2010, **11**, 2919–2926.
11 L. C. Arruda, M. Magaton, R. E. S. Bretas and M. M. Ueki, *Polym. Test.*, 2015, **43**, 27–37.
12 T. Zhang, W. Han, C. Zhang and Y. Weng, *Polym. Degrad. Stab.*, 2021, **183**, 109455.

13 M. Nofar, D. Sacligil, P. J. Carreau, M. R. Kamal and M. C. Heuzey, *Int. J. Biol. Macromol.*, 2019, **125**, 307–360.
14 N. Mallegni, T. V. Phuong, M. B. Coltelli, P. Cinelli and A. Lazzeri, *Materials*, 2018, **11**, 148.
15 C. Diaz, H. Y. Pao and S. Kim, *J. Appl. Packag. Res.*, 2016, **8**, 43–51.
16 C. Deetuam, C. Samthong, P. Pratumpol and A. Somwangthanaroj, *Iran. Polym. J.*, 2017, **26**, 615–628.
17 C. Zhang, T. Zhai, L.-S. Turng and Y. Dan, *Ind. Eng. Chem. Res.*, 2015, **54**, 9505–9511.
18 H. Tsuji, T. Yamada, M. Suzuki and S. Itsuno, *Polym. Int.*, 2003, **52**, 269–275.
19 L. Gardella, M. Calabrese and O. Monticelli, *Colloid Polym. Sci.*, 2014, **292**, 2391–2398.
20 M. Ma, H. Zheng, S. Chen, B. Wu, H. He, L. Chen and X. Wang, *Polym. Int.*, 2016, **65**, 1187–1194.
21 A. Fernández-Tena, I. Otaegi, L. Irusta, V. Sebastián, G. Guerrica-Echevarria, A. J. Müller and N. Aranburu, *Macromol. Mater. Eng.*, 2023, **308**, 2300213.
22 H. Jeong, J. Rho, J.-Y. Shin, D. Y. Lee, T. Hwang and K. J. Kim, *Biomedical Engineering Letters*, 2018, **8**, 267–272.
23 R. Muthuraj, M. Misra and A. K. Mohanty, *J. Appl. Polym. Sci.*, 2018, **135**, 45726.
24 I. Fortelny, A. Ujcic, L. Fambri and M. Slouf, *Frontiers in Materials*, 2019, **6**, 206.
25 S. Solechan, A. Suprihanto, S. A. Widyanto, J. Triyono, D. F. Fitriyana, J. P. Siregar and T. Cionita, *Materials*, 2022, **15**, 7396.
26 M. Eryildiz, A. Karakus and M. Altan Eksi, *J. Mater. Eng. Perform.*, 2024, 1–12.
27 B. Yao, Y. Zhu, Z. Xu, Y. Wu, L. Yang, J. Liu, J. Shang, J. Fan, L. Ouyang and H. S. Fan, *Polym. Eng. Sci.*, 2023, **63**, 3743–3761.
28 S. Murali, A. Agirre, L. Irusta, A. González and R. Tomovska, *Polymer*, 2023, **287**, 126421.
29 A. Ostafinska, I. Fortelný, J. Hodan, S. Krejčíková, M. Nevoralová, J. Kredatusová, Z. Kruliš, J. Kotek and M. Šlouf, *J. Mech. Behav. Biomed. Mater.*, 2017, **69**, 229–241.
30 M. Safari, A. Mugica, M. Zubitur, A. Martínez de Ilarduya, S. Muñoz-Guerra and A. J. Müller, *Polymers*, 2020, **12**, 17.
31 A. Fernández-Tena, R. A. Pérez-Camargo, O. Coulembier, L. Sangroniz, N. Aranburu, G. Guerrica-Echevarria, G. Liu, D. Wang, D. Cavallo and A. J. Müller, *Macromolecules*, 2023, **56**, 4602–4620.
32 A. T. Lorenzo, M. L. Arnal, J. Albuerne and A. J. Müller, *Polym. Test.*, 2007, **26**, 222–231.
33 H. Bai, H. Xiu, J. Gao, H. Deng, Q. Zhang, M. Yang and Q. Fu, *ACS Appl. Mater. Interfaces*, 2012, **4**, 897–905.
34 J. Chen, C. Deng, R. Hong, Q. Fu and J. Zhang, *J. Polym. Res.*, 2020, **27**, 1–11.
35 L. Cabedo, J. Luis Feijoo, M. Pilar Villanueva, J. M. Lagarón and E. Giménez, in *Macromolecular Symposia*, Wiley Online Library, 2006, vol. 233, pp. 191–197.
36 J. Urquijo, S. Dagréou, G. Guerrica-Echevarría and J. I. Eguiazábal, *J. Appl. Polym. Sci.*, 2016, **133**, 43815.
37 D. Sanchez Aldana, E. Duarte Villa, M. De Dios Hernández, G. González Sánchez, Q. Rascon Cruz, S. Flores Gallardo, H. Pinon Castillo and L. Ballinas Casarrubias, *Polymers*, 2014, **6**, 2386–2403.
38 W. A. Herrera-Kao, M. I. Loría-Bastarrachea, Y. Pérez-Padilla, J. V Cauich-Rodríguez, H. Vázquez-Torres and J. M. Cervantes-Uc, *Polym. Bull.*, 2018, **75**, 4191–4205.
39 T. Elzein, M. Nasser-Eddine, C. Delaite, S. Bistac and P. Dumas, *J. Colloid Interface Sci.*, 2004, **273**, 381–387.
40 K. Phillipson, J. N. Hay and M. J. Jenkins, *Thermochim. Acta*, 2014, **595**, 74–82.
41 J. R. Flores-León, D. E. Rodríguez-Félix, J. M. Quiroz-Castillo, H. Burrola-Núñez, M. M. Castillo-Ortega, J. C. Encinas-Encinas, J. Alvarado-Ibarra, H. Santacruz-Ortega, J. L. Valenzuela-García and P. J. Herrera-Franco, *ACS Omega*, 2024, **9**, 9526–9535.
42 I. Navarro-Baena, V. Sessini, F. Dominici, L. Torre, J. M. Kenny and L. Peponi, *Polym. Degrad. Stab.*, 2016, **132**, 97–108.
43 E. Ikada, *J. Photopolym. Sci. Technol.*, 1997, **10**, 265–270.
44 L. Aliotta, P. Cinelli, M. B. Coltelli, M. C. Righetti, M. Gazzano and A. Lazzeri, *Eur. Polym. J.*, 2017, **93**, 822–832.
45 B. Wunderlich, *Macromolecular Physics. Vol. 1: Crystal Structure Morphology, Defects*, Academic Press, 1973.
46 B. Crist and J. M. Schultz, *Prog. Polym. Sci.*, 2016, **56**, 1–63.
47 D. Cavallo and A. J. Müller, *Macromolecular Engineering: from Precise Synthesis to Macroscopic Materials and Applications*, 2022, pp. 1–57.
48 A. Fernández-Tena, G. Guerrica-Echevarria, N. Aranburu, Z. Wang, D. Cavallo and A. J. Müller, *ACS Appl. Polym. Mater.*, 2023, **6**, 583–595.
49 P. J. Lemstra, J. Postma and G. Challa, *Polymer*, 1974, **15**, 757–759.
50 M. R. Tant and W. T. Culberson, *Chem. Lett.*, 1999, **33**, 1152–1156.